Journal of the European Ceramic Society 21 (2001) 399–408

www.elsevier.com/locate/jeurceramsoc

Sol–gel preparation and characterization of manganese-substituted superconducting $YBa_2(Cu_{1-x}Mn_x)_4O_8$ compounds

A. Baranauskas [a], D. Jasaitis [a], A. Kareiva [a,*], R. Haberkorn [b], H.P. Beck [b]

[a] *Department of General and Inorganic Chemistry, Vilnius University, Naugarduko 24, LT-2006 Vilnius, Lithuania*

[b] *Institute of Inorganic and Analytical Chemistry and Radiochemistry, Saarland University, Im Stadtwald, D-66041 Saarbruecken, Germany*

Received 29 June 2000; accepted 2 August 2000

Abstract

In this work the effect on the structural and superconducting properties of $YBa_2Cu_4O_8$ (Y-124) of replacing Cu by Mn was studied. Multimetallic oxide powders with the composition of $YBa_2(Cu_{1-x}Mn_x)_4O_8$ ($x=0.00$, 0.01, 0.02, 0.03, 0.04 and 0.05) have been prepared by a simple aqueous sol–gel method at an oxygen pressure of 1 atm starting from an aqueous mixture of the metal acetates. Homogeneous gels were achieved by complexing copper ions by tartaric acid before the gelation process. Thermal decomposition of the gels was studied by thermogravimetry. Effects of manganese substitutions on the properties of compounds were studied by X-ray powder diffraction, TG analysis, IR spectroscopy and resistivity measurements. These data indicated that the transition temperature of superconductivity drastically decreases upon Mn substitution, and that superconductivity is lost at 3% of Mn substitution level. XRD measurements showed that the structure of the Y-124 phase is also largely affected even at low manganese-substitutional levels.

Keywords: Oxide superconductors; Sol–gel processes; Substitution effects; Superconductivity; $YBa_2Cu_4O_8$

1. Introduction

The search for high-temperature superconductivity and novel superconducting mechanisms is one of the most challenging tasks of condensed-matter physicists as well as material scientists.[1–3] The studies on various substitutions in oxide superconducting systems have proven to be of great importance since changes in the critical transition temperature (T_C) are usually observed. For example, the effects of non-isovalent substitutions for Y in the YBCO superconductors have attracted a great deal of attention in the past.[4,5] Results show that, basically, such doping can vary the hole concentration in a controlled manner influencing the superconducting properties of the material obtained. Doping of different ions at the copper sites in YBCO superconductors serves as a useful diagnostic probe to investigate the role of different copper sites in the occurrence of superconductivity in these superconductors.[6–8] In almost all such cases, the destabilization of YBCO superconducting phases and consequently the degradation of superconductivity in these compounds have been determined at a low substitutional level.

The $YBa_2Cu_4O_8$ (Y-124) superconducting compound is thermodynamically stable and stoichiometric. The orthorhombic-to-tetragonal phase transition observed in the $YBa_2Cu_3O_7$ (Y-123) phase is absent, and thus Y-124 is an ideal system to study different substitution effects.[9,10] For most of the multimetallic oxides the physical and chemical properties depend largely on impurities and dopants, besides the compositional homogeneity, phase purity, surface morphology or microstructure.[11,12] These features, crucial for the preparation of electronic, optic, and catalytic materials, are dependent on the method of synthesis. Recently we described the use of an aqueous sol–gel method for the synthesis of monophasic non-substituted $YBa_2Cu_4O_8$,[13,14] as well as superconducting Y-124 samples substituted in the yttrium position by Eu[15] and Ca,[16] in the barium position by Sr,[17] in the copper position by Fe,[15] Co and Ni.[18] To date, no systematic studies have been reported on manganese substitution in the $YBa_2Cu_4O_8$ superconductor, to our knowledge. Such investigations are very interesting from the theoretical point of

* Corresponding author. Tel.: +370-2-336214; fax: +370-2-330987.

E-mail address: aivaras.kareiva@chf.vu.lt (A. Kareiva).

0955-2219/01/$ - see front matter
PII: S0955-2219(00)00206-5

view taking into account some common features of appropriate metal ions. Manganese is roughly similar to iron in its physical and chemical properties. The common and most stable oxidation state of manganese is the divalent one, and both the elements Mn(II) and Fe(III) are magnetically similar, since the high-spin d^5 electron configuration is the same for Mn(II) and for Fe(III). Due to the above mentioned similarities, the destabilisation of the Y-124 superconducting phase by substituting Cu by Mn would be expected, as was observed in the case of iron-substituted samples. Although Mn(II) is the most stable oxidation state, it might be oxidized quite readily. Therefore, the situation might be different if the manganese oxidation state increased up to +4 during final annealing of the material in the oxidizing atmosphere. It is well known that the higher and lower manganese oxides can be interconverted by changing the temperature and oxygen partial pressure, via formation of intermediate oxides, such as Mn_2O_3 or Mn_3O_4. In this case, a non-isovalent substitution in the Y-124 superconducting phase is possible, which eventually causes changes in the charge carrier concentration, consequently influencing the physical properties of the superconductor. On the other hand, Er et al.[19] have recently confirmed that Mn at higher valence states may form Mn(III)/Mn(IV) donor pairs with a high ability for electron trapping.

The above mentioned considerations have initiated the present work, motivating us to continue our earlier investigations on the substitution effects in the $YBa_2Cu_4O_8$ superconductor. In the work described herein, we present a systematic study of Mn substitution effects in the $YBa_2(Cu_{1-x}Mn_x)_4O_8$ system. The precursor gel powders and the final synthesis products were characterized by X-ray powder diffraction analysis, thermal analysis, IR spectroscopy and resistivity measurements.

2. Experimental

2.1. Characterization

The synthesized samples were characterized by X-ray powder analysis performed with a D5000 (Siemens, Germany) diffractometer, using Cu$K\alpha_1$ radiation. For IR studies, a Perkin–Elmer FT-IR Spectrum BX II apparatus was used. The samples were mixed (1.5%) with dried KBr and pressed into pellets. Thermal analysis (TG/DTA) of synthesized gel precursors was performed on a simultaneous STA 409 thermal analyzer (Netzsch, Germany). The thermal decomposition of the gels in flowing air was studied in the temperature range 20–1100°C using a heating rate of 5°C/min. The sample weight was 10–20 mg. With some of the TG measurements simultaneous evolved gas analysis (EGA–MS) curves were recorded by means of a coupled mass analyzer (Balzers, Germany). Also, the oxygen stability of the final products under oxygen atmosphere was investigated by TG measurements (heating rate 5°C/min; sample weight 25–30 mg). A standard four-probe technique was used to measure the temperature dependence of the resistivity in the range 20–300 K.

2.2. Synthesis

The $YBa_2(Cu_{1-x}Mn_x)_4O_8$ samples with $x = 0.00$, 0.01, 0.02, 0.03, 0.04 and 0.05 were prepared by an acetate–tartrate sol–gel method developed previously for the synthesis of the pure $YBa_2Cu_4O_8$ superconductor.[13,14] As starting compounds stoichiometric amounts of Y_2O_3, $Cu(CH_3COO)_2.H_2O$, $Ba(CH_3COO)_2$ and $Mn(CH_3COO)_2$, all of them analytical grade, were used. In the sol–gel process Y_2O_3 or Y first was dissolved in 0.2 M acetic acid at 55–60°C. Next, $Ba(CH_3COO)_2$ and $Cu(CH_3COO)_2.H_2O$ or appropriate mixtures of $Mn(CH_3COO)_2$ and $Cu(CH_3COO)_2.H_2O$, all of them dissolved in a small amount of distilled water, were added with intermediate stirring during several hours at the same temperature. A solution of tartaric acid in water was added to adjust the pH to 5.6, thus preventing crystallization of copper acetate during gelation. The obtained solution was concentrated during about 8 h at 60–65°C in an open beaker. Under continuous stirring the transparent blue gel formed. After further drying in an oven at 80°C fine grained blue powders were obtained. The precursor powders were calcined for 10 h at 820°C in flowing oxygen, reground in an agate mortar, and again heated for 20 h at 820°C reground, pelletized and annealed for 20 h at 820°C in a flowing oxygen atmosphere at ambient pressure.

3. Results and discussion

3.1. Synthesis and characterization of the precursors

A rapid development of multinary metal oxide ceramic materials, which are produced from fine-grained synthetic powders using new technologies, has to a large extent revolutionized both concepts and technology in the ceramic field. The sol–gel processing route to advanced glasses and ceramics is a way of manipulating molecular precursors to form bulk oxide materials. Moreover, the sol–gel synthesis methods based on molecular precursors have a decisive advantage over the other solution routes because they allow chemical interactions among the initial mixture of precursor species favouring the evolution of the solid-state structure at the atomic level.[20–22] A series of $YBa_2(Cu_{1-x}Mn_x)_4O_8$ ($x = 0.00$, 0.01, 0.02, 0.03, 0.04 and 0.05) samples were prepared by an acetate–tartrate sol–gel method developed previously for the synthesis of the pure YBa_2-

Cu_4O_8 superconductor.[13,14] As starting compounds stoichiometric amounts of Y_2O_3 or metallic Y, $Cu(CH_3COO)_2.H_2O$, $Mn(CH_3COO)_2$, and $Ba(CH_3COO)_2$, all of them analytical grade, were used. In the sol–gel process appropriate amounts of Y_2O_3 or metallic Y were first dissolved in 0.2 M acetic acid at 55–60°C. Next, $Ba(CH_3COO)_2$ and appropriate mixtures of $Cu(CH_3COO)_2.H_2O$ and $Mn(CH_3COO)_2$, all of them dissolved in a small amount of distilled water, were added with intermediate stirring during several hours at the same temperature. A solution of tartaric acid in water was added to adjust the pH to 5.6, thus preventing crystallization of copper acetate during gelation. The obtained solution was concentrated in an open beaker and under continuous stirring until it became a transparent blue gel. The precursor powders were dried and calcined in flowing oxygen; see Experimental Section. A schematic diagram of the processing steps involved in the preparation of the manganese-substituted Y-124 samples is shown in Fig. 1. To demonstrate the suitability and versatility of our sol–gel approach to the synthesis of manganese-substituted Y-124 compounds, we have chosen two starting materials, Y_2O_3 and metallic Y, as yttrium source. The choice was based upon minimum cost and maximum availability. The results of characterization of precursor gels and final oxide ceramics for the two different synthesis routes (whether Y_2O_3 or metallic Y was used) were approximately the same.

The main requirement for the sol–gel approach is to achieve a very high level of precursor homogeneity to hopefully give an excellent homogeneity in the final ceramic material. Thus special attention was paid to the powder X-ray diffraction studies of the precursor gels. The XRD patterns of the Y-Ba-Cu-O and Y-Ba-Cu(Mn)-O acetate–tartrate gels were recorded in the region of $2\theta = 20$–$70°$. The diffraction patterns of the powders obtained were broad due to the amorphous character of the systems synthesized. If the conditions of the sol–gel process are not completely optimized a partial crystallization of initial metal salts may proceed.[23] However, no peaks whatsoever due to crystallization of metal acetates or tartrates, or crystallization of any undesired or contaminating phase could be identified for both Y-Ba-Cu-O and Y-Ba-Cu(Mn)-O precursor gels. The XRD patterns of all gels only indicated a broad unidentified amorphous hump around $2\theta = 35°$. During calcination and final heat treatment of such homogeneous precursors monophasic nanosized multimetallic oxides can be obtained.

Infrared (IR) spectra of the Y-Ba-Cu-O gel and substituted Y-Ba-Cu(Mn)-O precursor gels were measured as well. The IR spectrum of a representative sample (gel with 3% of Mn substitution level) is presented in Fig. 2. This type of IR spectrum was qualitatively the same regardless of manganese substitution level. According to

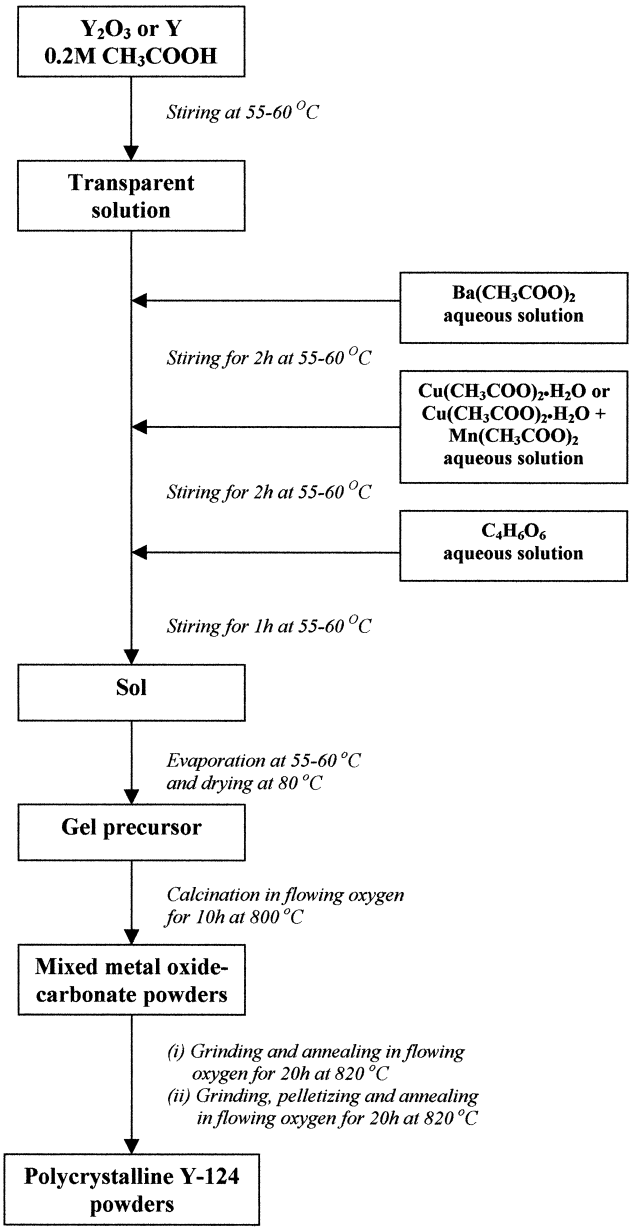

Fig. 1. Scheme of the steps involved in the sol–gel process used for the synthesis of manganese-doped $YBa_2Cu_4O_8$ superconductors.

the origin of the bands, this spectrum may be divided into four regions: 3750–2700, 1850–1200, 1150–825 and 800–515 cm^{-1}. The absorptions at ca 3100–2800 and 1430–1410 cm^{-1} are due to stretch vibrations in CH_3 and CH_2; strong bands at 3400–3200 and 1100–1000 cm^{-1}, and medium bands at 1300–1200 cm^{-1} are probably due to CH–OH stretching; the strong bands due to CO–OH stretching can be identified at 3500–3200 cm^{-1}, 1700–1550 and 1350–1340 cm^{-1}, as well as at the medium bands at 950–800 cm^{-1}. But since both CH_3 and CH–OH stretchings were identified we suppose that both acetate and tartrate ligands are in the coordination sphere of metals.

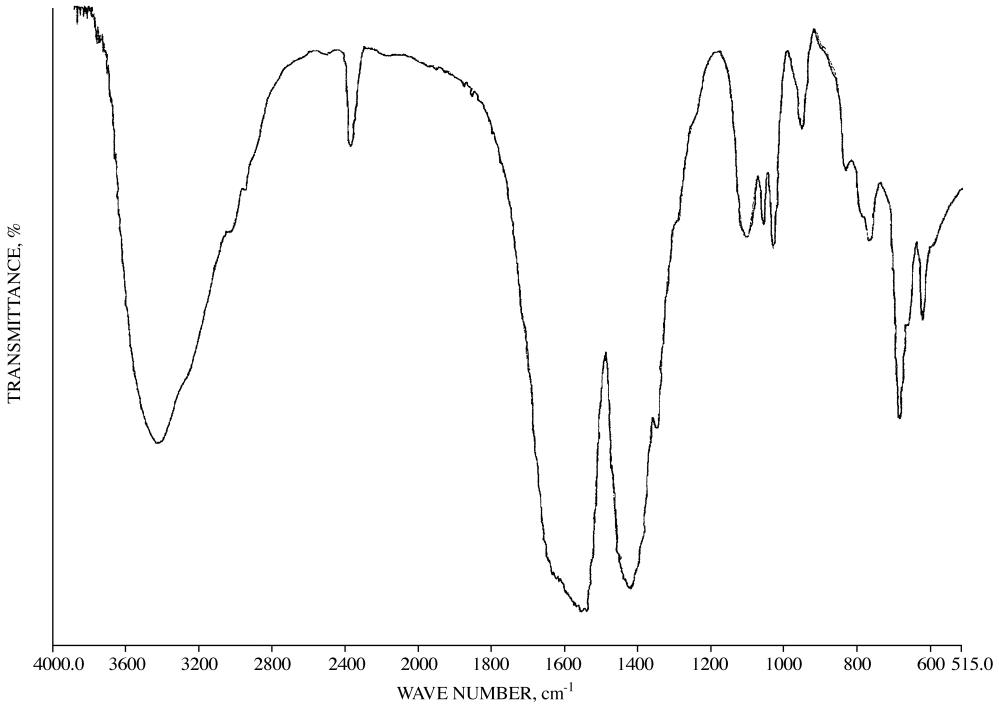

Fig. 2. IR spectrum of the Y-Ba-Cu(Mn)-O acetate–tartrate gel with 3% Mn substitutional level.

A broad absorption in the spectrum of the precursor gels around 3400 cm^{-1} also indicates the presence of adsorbed water.[24] In addition, broad and multiple absorptions in the range 3700–3400 cm^{-1} can be assigned to a metal-bound hydroxide group.[25] Therefore, taking into account that low-valent cations ($z < +4$) give rise to aquo–hydroxo and/or hydroxo complexes over the whole range of pH,[26,27] the process of gelation in the system investigated probably occurs via the olation mechanism. Basically it corresponds to a nucleophilic substitution in which M–OH or complexing ligands are nucleophiles and H_2O is a leaving group. In the 800–515 cm^{-1} region of the IR spectrum the observed specific peaks at 764, 681, 662 and 618 cm^{-1} may be attributed to characteristic M–O vibrations.[28]

It is well known that thermal characterization of synthesized samples is important both for control of the reaction process and of the properties of materials obtained. In this context, thermal analysis is a versatile group of techniques which can be used to aid preparative studies.[11,29–33] The mechanism of the thermal decomposition of the dried gels was studied by TG/DTA measurements from 20 to 1100°C using a heating rate of 5°C/min. The TG/DTA curves for Y-Ba-Cu-O acetate–tartrate gels are shown in Fig. 3. The TG curve shows three main weight losses in the temperature range 20–180 (6.98%), 190–270 (22.30%) and 270–405°C (9.14%). The weight loss below 175°C is due to the evaporation of water and solvent molecules. The two following and most significant decomposition steps can be attributed to the pyrolysis of organic compounds and the degradation of intermediate species formed during the gelation process. In the temperature range 190–270°C mainly the copper constituent decomposes, and above 270°C the final decomposition of the gel proceeds via homogeneously distributed intermediate species.[13] The TG measurements clearly show that the decomposition behaviour of the gel differs considerably depending on the starting materials, yttrium acetate, barium acetate, and copper acetate.[13,34] For example, the decomposition of anhydrous copper acetate occurs around 250°C, which is higher than the decomposition temperature of an acetate–tartrate copper gel. The decomposition of $Ba(CH_3COO)_2$ to $BaCO_3$ occurs approximately at 420°C. On the other hand, the decomposition of the barium acetate–tartrate gel occurs in three steps, the main decomposition occurring between 280 and 345°C. In the case of $Y(CH_3COO)_3.H_2O$, the dehydration process starts at 80°C; the resulting anhydrous yttrium acetate is stable up to 300°C ($Y_2O_2CO_3$ is also likely to be formed at this temperature), which decomposes to the oxide above 600°C. Again, thermal decomposition of yttrium acetate–tartrate gels is quite different. The results obtained once more confirm that individual chemical species with complicated structures are formed during the gelation process.

The thermal decomposition behaviour is associated with endothermic and exothermic effects in the DTA curve. The first decomposition step due to desorption of water corresponds to a broad endothermic peak around 100°C on the DTA curve. Exothermic peaks around

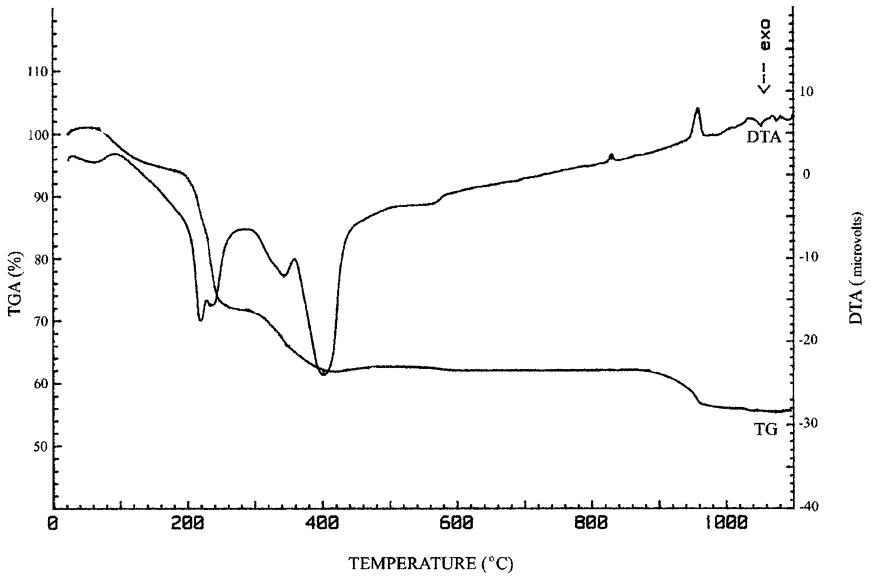

Fig. 3. TG/DTA curves for the Y-Ba-Cu-O acetate–tartrate gel recorded in a flowing air atmosphere. The heating rate was 5°C/min.

219, 233, 344 and 401°C on the DTA curve are indications of the pyrolysis processes which take place during further heating of the gel. The final weight loss on the TG curve observed in the temperature range 820–960°C (6.08%) is accompanied by a weak endothermic peak around 830°C and a more intensive endothermic peak at 958°C. The nature of these peaks is not sufficiently clear. We can postulate that these peaks correspond to the beginning of the $YBa_2Cu_4O_8$ crystallization process and accompanying structural transformations.[35] Moreover, probably at this temperature the remaining $BaCO_3$ undergoes an endothermic decarbonation reaction to BaO (which simultaneously reacts with other oxides) and carbon oxide is released. The nature of the endothermic peak at 958°C in the DTA curve can be associated with the decomposition of Y-124 particles to Y-123 and CuO phases.[36] Finally, weak exothermic peaks above 1020°C can be attributed to the melting of formed products. Thus, the results of thermal decomposition of gels are also useful for the determination of the optimum conditions of final annealing of precursor powders to obtain superconducting materials. It should be noted that the decomposition mechanism is approximately the same as that for the Y-Ba-Cu(Mn)-O precursor gels.

To assist in the interpretation of the thermal decomposition mechanism of the precursor gels simultaneous evolved gas analyses (EGA–MS) were performed with some of the TG measurements by means of a coupled mass analyzer. In Fig. 4 the TG and EGA–MS curves for the representative sample of Y-Ba-Cu(Mn)-O precursor gel are shown. Apparently, the observed evolution of CO_2 and H_2O in the temperature ranges of weight losses confirms our considerations concerning the mechanism of thermal decomposition of the precursor gels.

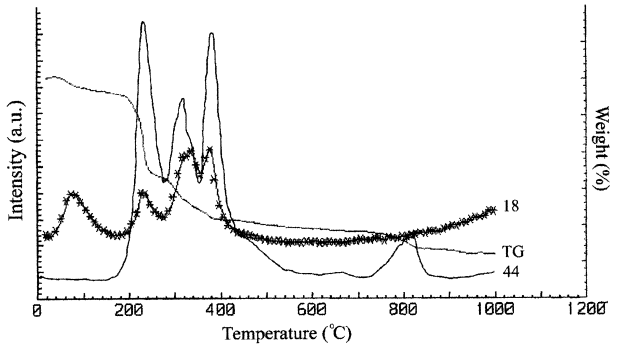

Fig. 4. Thermal decomposition of the Y-Ba-Cu(Mn)-O acetate–tartrate gel with 5% Mn substitutional level under a flowing air atmosphere, monitored by TG and EGA–MS (the mass numbers are indicated). The heating rate was 5°C/min.

3.2. Characterization of the heat-treated precursors

Resistivity measurements performed on as-prepared Y-124 samples showed a sharp superconducting transition with T_C (onset) = 79 K and T_C (zero) = 67 K (Fig. 5). As seen, with manganese substitutions in small concentrations up to 2%, the effect on superconductivity is, however, deleterious with T_C getting suppressed drastically at a rate of about 19 K per%. From Fig. 5 the following features of T_C suppression in the Y-124 system became clear.

1. The onset critical temperature of superconductivity decreased down to 62.5 K for $YBa_2(Cu_{0.99}Mn_{0.01})_4O_8$ [T_C (zero) = 49 K], and down to 41 K for $YBa_2(Cu_{0.98}Mn_{0.02})_4O_8$ [T_C (zero) =

23 K], the transition range becoming broader with increasing substitution.
2. The $YBa_2(Cu_{1-x}Mn_x)_4O_8$ samples with $x \geqslant 0.03$ exhibited only semiconducting behaviour indicating the loss of superconductivity at 3% Mn doping.
3. The resistivity in the normal conducting state increases with the number of Mn dopant sites which probably act as dissipation centres for electron transport.

The more dramatic manganese substitution effect on T_C compared with Fe-substituted Y-124 samples was rather unexpected. Fig. 6 summarizes previously published T_C suppression data for Fe[37] and for Mn in the Y-124 compound synthesized by the aqueous sol–gel

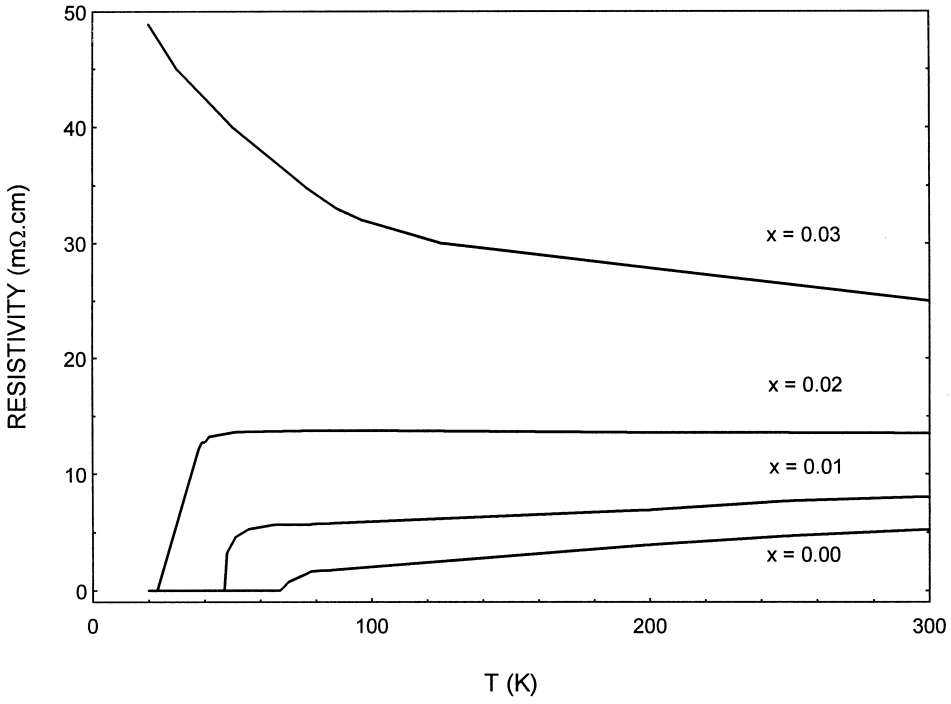

Fig. 5. Resistivity vs temperature for the series of samples of $YBa_2(Cu_{1-x}Mn_x)_4O_8$ with different values of x.

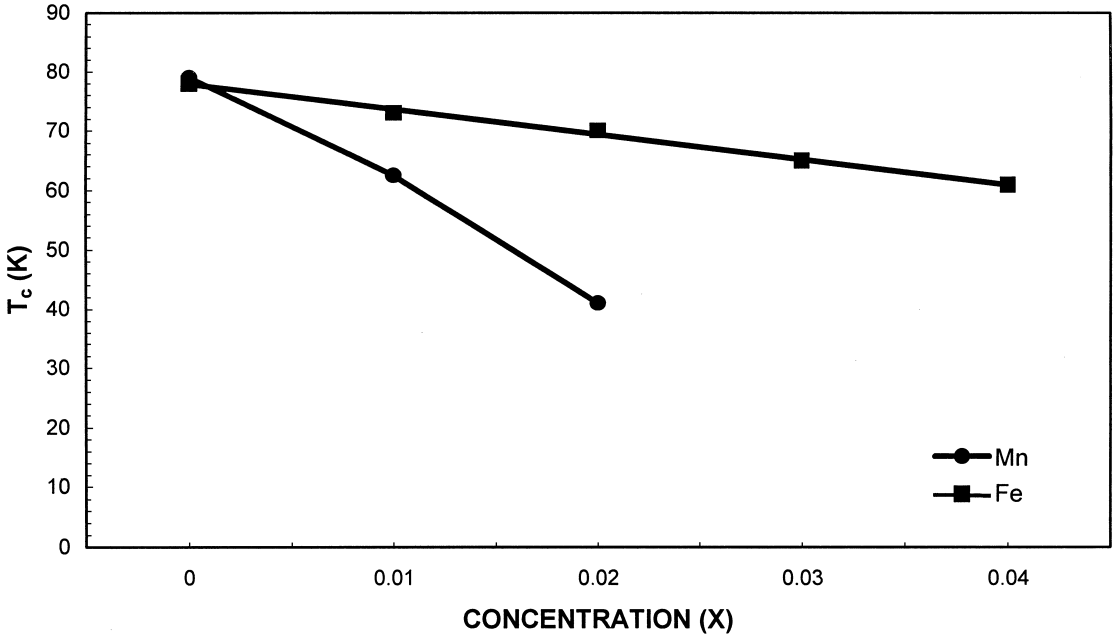

Fig. 6. Degradation of T_C (onset) of the Y-124 superconductor with doping of Mn and Fe. T_C values for iron-substituted samples as previously determined.

method. As seen, superconducting properties of iron-substituted Y-124 phase are lost much slower (at a rate of about 4 K percent) indicating a weaker effect of Fe. It was previously demonstrated through Mössbauer studies[37] that iron preferentially enters Cu(2) plane sites in Y-124. Thus, this fact led us to speculate that manganese may occupy Cu(1) chain sites or both Cu(1) and Cu(2) sites in the Y-124 system.[38] It is obvious that Mn substitution brings about the evident decrease of T_C of $YBa_2(Cu_{1-x}Mn_x)_4O_8$, but the important question concerning the reasons for such an effect is yet to be answered.

In Fig. 7 the XRD patterns of the $YBa_2(Cu_{1-x}Mn_x)_4O_8$ samples are presented. Because of the structural similarities, the greater part of X-ray diffractions of Y-123, Y-124 and Y-247 phases coincide, which makes it extremely difficult to distinguish them on the basis of their XRD patterns alone. Thus, to facilitate the interpretation of XRD patterns of the synthesized $YBa_2(Cu_{1-x}Mn_x)_4O_8$ samples, we included a comparison of the XRD patterns of superconducting Y-123, Y-124 and Y-247 phases (Fig. 8). The XRD patterns of the manganese-substituted Y-124 samples, however, showed considerable changes upon increasing substitution. According to X-ray diffraction analysis only traces of Y-123 and minor amounts of Y-211 were present as impurity phases in the non-doped $YBa_2Cu_4O_8$ sample (see Fig. 7a). The Y-124 spectrum can also be identified in the 1% Mn sample. However, peak intensities of the impurity phases increased with increasing Mn content up to $x=0.2$. On further increasing the substitution level a main peak in the XRD patterns of these samples can already be attributed to the impurity phase. Starting from 3% substitution, characteristic features of the

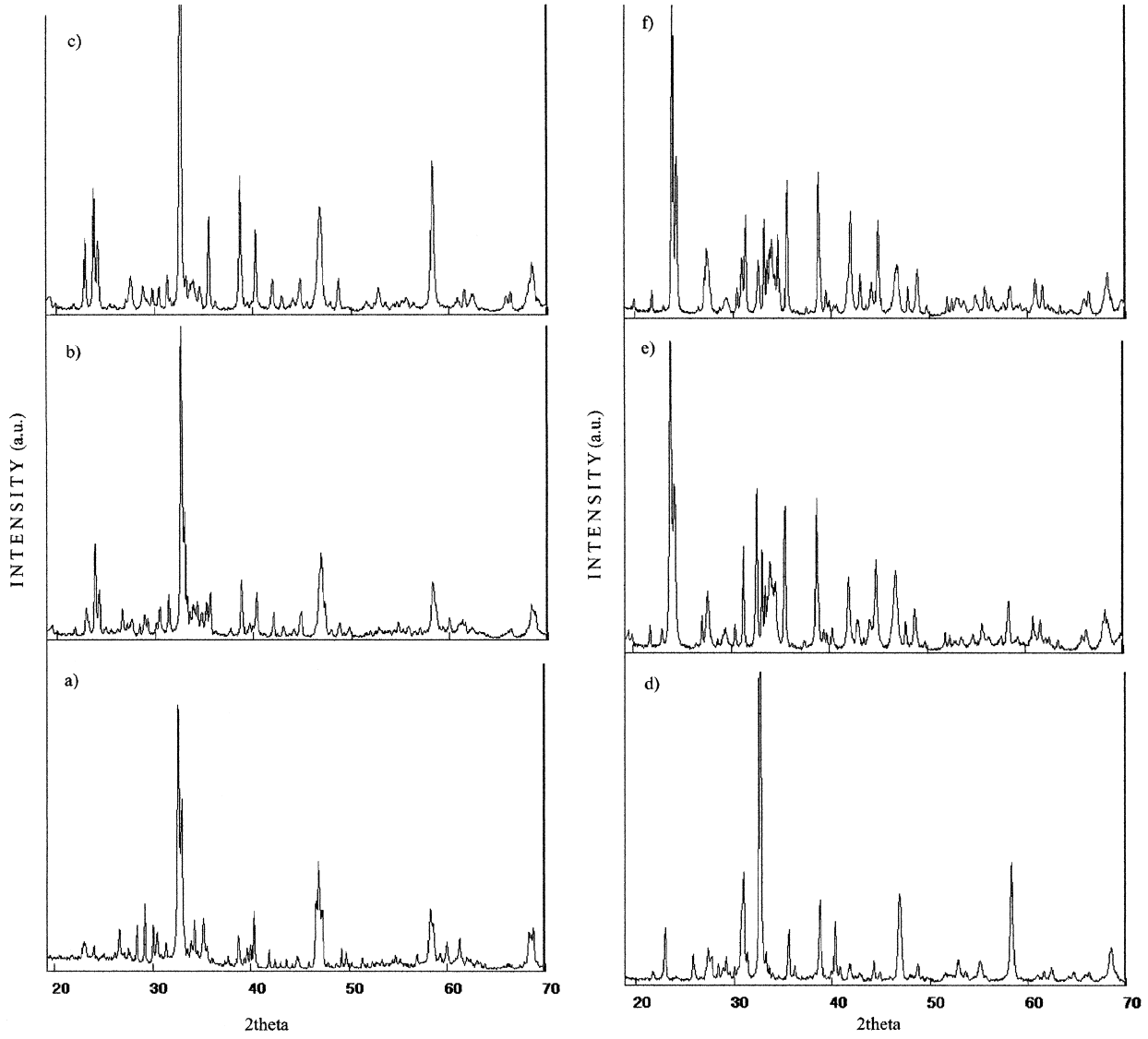

Fig. 7. Powder X-ray diffraction patterns of the $YBa_2(Cu_{1-x}Mn_x)_4O_8$ samples: (a) $x=0.00$; (b) $x=0.01$; (c) $x=0.02$; (d) $x=0.03$; (e) $x=0.04$; (f) $x=0.05$.

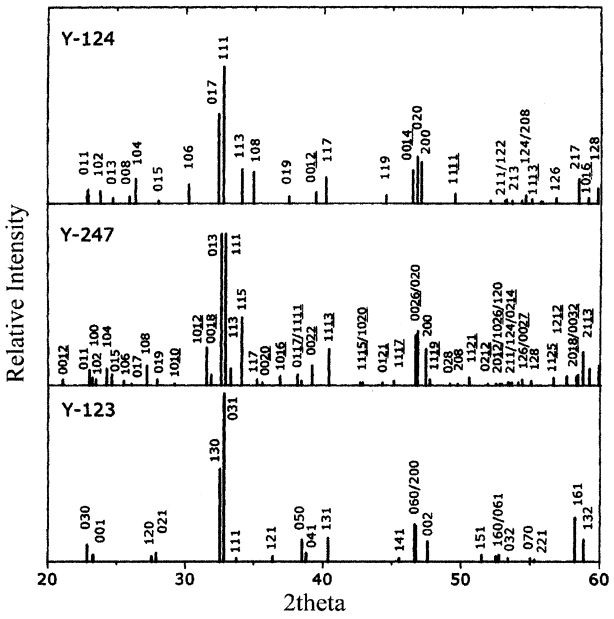

Fig. 8. Schematic presentation of the XRD patterns and Miller indices of Y-124, Y-247, and Y-123 phases from JCPDS© 1991 and 1996 reference data.

orthorhombic Y-124 diffraction pattern already vanish: the intensity of the (113) and (108) diffractions at $2\theta \cong 34.4$ and 35.8° decreases strongly and the splitting of the (200) (020) (0014) at $2\theta \cong 47°$ and the (017) (111) diffractions at $2\theta \cong 33°$ vanishes. Moreover, in the case of $x = 0.4$ and $x = 0.5$, peaks due to the Y-124 phase have disappeared. The approximate phase compositions of the synthesized samples roughly estimated according to XRD analysis are presented in Table 1.

As already mentioned, we have previously reported about iron substitution effects in the $YBa_2Cu_4O_8$ superconductor synthesized by the sol–gel technique. It is interesting to note that iron doping destabilizes the Y-124 phase favouring the formation of the tetragonal $YBa_2Cu_3O_{7-\delta}$. The peaks due to the Y-123 structure were clearly seen in the XRD patterns recorded for the $YBa_2(Cu_{1-x}Fe_x)_4O_8$ samples with x equal to or larger than 0.04.[37] Similar results were obtained when investigating the effect of Ni and Co substitution in Y-124 prepared by the acetate–tartrate sol–gel method.[18] Both Ni and Co substitutions strongly changed the superconducting properties of the Y-124 superconductor, however the structure was again less dramatically affected in comparison with Mn substitution. We can conclude, that substitution of Mn in the copper positions (possibly at the Cu(1) square planar fourfold coordinated chain sites) of Y-124 drastically influences the formation of $YBa_2Cu_4O_8$ phase. This can be explained perhaps only by the difference of ionic radii of the metals, which are 0.57 Å for copper and 0.67 Å for manganese. For example, the ionic radii for iron, cobalt and nickel are 0.63, 0.58, and 0.55 Å, respectively. As seen, the difference in the ionic radii of copper and dopant elements is the largest for the Mn case. These are the conclusions that can be drawn from the XRD measurements.

Also, in order to detect small amounts of Y-123 and Y-247 impurities the differences in the stability towards oxygen might be taken into account. For instance, the Y-123 phase starts to lose the Cu–O chain oxygen around 300–400°C.[39] When the Y-247 phase is heated in an oxidizing atmosphere, it shows a reversible weight loss between 570 and 850°C due to release of oxygen from the single Cu–O chains in the Y-123 blocks.[40] On the other hand, the Y-124 phase exhibits an excellent thermal stability up to 670–700°C in an inert atmosphere, up to 830°C in air and up to 860–890°C in oxygen atmosphere.[9,16,31,41,42] Thus, the phase purity of the three purest samples has also been checked by TG measurements.

Fig. 9 shows the TG curves for heating under oxygen atmosphere for the $YBa_2Cu_4O_8$, $YBa_2(Cu_{0.99}Mn_{0.01})_4O_8$, and $YBa_2(Cu_{0.98}Mn_{0.02})_4O_8$ samples. No indication of weight loss could be seen below ~890°C in the oxygen atmosphere for a non-doped Y-124 sample. Such an observation again indicates that the $YBa_2Cu_4O_8$ sample mainly contains pure Y-124, which is in a good agreement with the XRD results. From Fig. 9 it can be also seen that incorporation of manganese in the Y-124 structure destabilizes the oxygen sublattice. The mass of manganese-substituted samples decreases continuously starting from approximately 300°C due to the loss of oxygen from the Y-123 impurity phase. Moreover, a slightly increased mass loss was detected in the temperature region of 500–800°C. In this region Y-247 exhibits oxygen loss. And in both cases the weight

Table 1
Phase composition of synthesized $YBa_2(Cu_{1-x}Mn_x)_4O_8$ samples according to XRD analysis data

Sample	Major phase	Secondary phases
$YBa_2Cu_4O_8$	Y-124	Traces of Y-123 and Y-211
$YBa_2(Cu_{0.99}Mn_{0.01})_4O_8$	Y-124	Y-123, Y247, CuO
$YBa_2(Cu_{0.98}Mn_{0.02})_4O_8$	Y-124	Y-123, Y-247, $BaCuO_2$, CuO
$YBa_2(Cu_{0.97}Mn_{0.03})_4O_8$	Y-123, Y-247	$Y_2Cu_2O_5$, Y_2BaCuO_5, $BaCuO_2$, CuO
$YBa_2(Cu_{0.96}Mn_{0.04})_4O_8$	–	$Y_2Cu_2O_5$, Y_2BaCuO_5, $BaCuO_2$, CuO, $BaCO_3$, Y_2O_3, unknown phases
$YBa_2(Cu_{0.95}Mn_{0.05})_4O_8$	–	Mixture of different polycrystalline phases

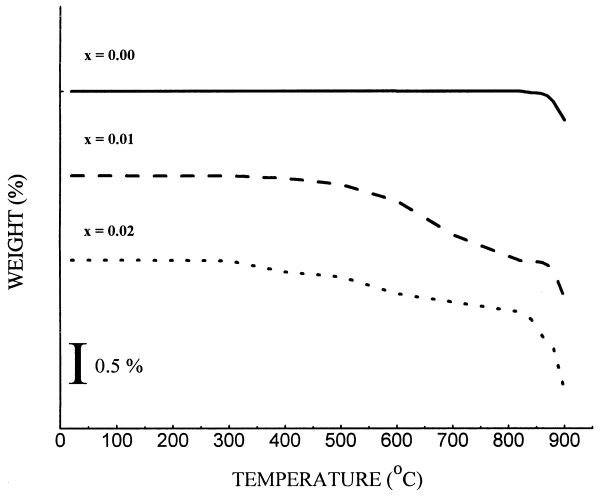

Fig. 9. Thermal stability curves in flowing oxygen atmosphere of $YBa_2Cu_4O_8$ (solid line), $YBa_2(Cu_{0.99}Mn_{0.01})_4O_8$ (broken line), and $YBa_2(Cu_{0.98}Mn_{0.02})_4O_8$ (dotted line). The heating rate was 5°C/min.

suddenly decreased around 850–860°C. The latter oxygen loss is likely to correspond to the decomposition of the Y-124 phase.[40] Thus, TG measurements in oxygen flow of manganese-substituted $YBa_2(Cu_{0.99}Mn_{0.01})_4O_8$ and $YBa_2(Cu_{0.98}Mn_{0.02})_4O_8$ samples confirmed unambiguously the presence of orthorhombic or tetragonal $YBa_2Cu_3O_{7-\delta}$ and $Y_2Ba_4Cu_7O_{15}$ impurity phases. These phases were detected by X-ray diffraction measurements (see Fig. 7) in the same samples, i.e. the obtained thermogravimetric results are consistent with the XRD results. Therefore, the reason for the decrease in T_C on substituting copper by manganese in Y-124 phase possibly could be attributed to such structural changes, which are mostly caused by the considerable difference in the ionic radius of the involved metals.

4. Conclusions

For the first time to our knowledge, manganese substituted superconducting $YBa_2(Cu_{1-x}Mn_x)_4O_8$ samples were synthesized by a simple aqueous sol–gel method. High homogeneity of the synthesized precursor gels were shown by XRD analysis, IR spectroscopy, and TG/DTA/EGA–MS measurements.

We have demonstrated that the critical temperature of superconductivity decreases dramatically from 79 K for the non-substituted sample, $YBa_2Cu_4O_8$, to 41 K for the sample with 2% of manganese substitutional level, $YBa_2(Cu_{0.98}Mn_{0.02})_4O_8$. The decrease of the transition temperature, as a result of the Mn substitution, cannot be explained directly, for instance, by magnetic pair breaking or destruction of the antiferromagnetic correlation of the Cu atoms in the planes.[6] According to the XRD analysis and stability measurements under controlled oxygen atmospheres, impurity phases, such as Y-123 and Y-247, have already formed in the samples with a 1 and 2% of manganese substitutional level under the usual preparation conditions. On further increasing the manganese substitutional level, peaks due to the Y-124 phase disappeared in the diffractograms. We draw the conclusion, that these structural changes are mostly caused by the considerable difference in the ionic radius of copper and manganese. However, a more detailed study of structural effects caused by manganese substitution should be performed.

Acknowledgements

A. Baranauskas is grateful for financial support from the Saarland University. The authors are indebted to N. Cetverikova for technical assistance.

References

1. Pedersen, K. R. and Jørgensen, J.-E., XANES study of rare-earth valency and 4f hybridization in $Pb_2Sr_2Ln_{1-x}Ca_xCu_3O_8$ for Ln = Ce, Pr and Tb. *Physica C*, 1996, **264**, 185–190.
2. Mook, H. A., Pengcheng, Dai, Dogan, F. and Hunt, R. D., One-dimensional nature of the magnetic fluctuations in $YBa_2Cu_3O_{6.6}$. *Nature*, 2000, **404**, 729–731.
3. Cava, R. J., Oxide superconductors. *Journal of the American Ceramic Society*, 2000, **83**, 5–28.
4. Gyurov, G., Khristova, I., Peshev, P. and Abrashev, M. V., Preparation of a calcium-substituted copper-rich yttrium barium copper oxide superconductor from a spray-dried nitrate precursor. *Materials Research Bulletin*, 1993, **28**, 1067–1074.
5. Zheng, X. G., Suzuki, M., Xu, C., Kuriyaki, H. and Hirakawa, K., Synthesis of Ca-substituted $Y_{1-x}Ca_xBa_2Cu_4O_8$ at ambient pressure using CuI. *Physica C*, 1996, **271**, 272–276.
6. Verma, M. and Tomar, V. S., Comparison of Co and Ni doping at copper sites in Y-124 high temperature superconductor. *Physica C*, 1996, **272**, 335–341.
7. Fujihara, S., Kozuka, H. and Yoko, T., Superconducting properties of the lithium-substituted $YBa_2Cu_4O_8$ prepared by the sol–gel method. *Journal of Materials Science*, 1996, **31**, 2975–2979.
8. Schwer, H., Karpinski, J., Kaldis, E., Meijer, G. I., Rossel, C. and Mali, M., Evidence for Al doping in the CuO_2 planes of $YBa_2Cu_4O_8$ single crystal. *Physica C*, 1996, **267**, 113–118.
9. Miyatake, T., Gotoh, S., Koshizuka, N. and Tanaka, S., T_C increased to 90 K in $YBa_2Cu_4O_8$ by Ca doping. *Nature*, 1989, **341**, 41–42.
10. Zhou, W., Xin, Y. and Jefferson, D. A., HRTEM surface profile imaging of superconducting $YBa_2Cu_4O_8$. *Journal of Solid State Chemistry*, 2000, **149**, 327–332.
11. MacKenzie, K. J. D. and Kemmitt, T., Evolution of crystalline aluminates from hybrid gel-derived precursors studied by XRD and multinuclear solid-state MAS NMR. II. Yttrium–aluminium garnet, $Y_3Al_5O_{12}$. *Thermochimica Acta*, 1999, **325**, 13–18.
12. Veith, M., Mathur, S., Lecerf, N., Huch, V., Decker, T., Beck, H. P., Eiser, W. and Haberkorn, R., Sol-gel synthesis of nano-scaled $BaTiO_3$, $BaZrO_3$ and $BaTi_{0.5}Zr_{0.5}O_3$ oxides via single-source alkoxide precursors and semi-alkoxide routes. *Journal of Sol-Gel Science and Technology*, 2000, **17**, 145–158.
13. Kareiva, A., Karppinen, M. and Niinistö, L., Sol–gel synthesis of superconducting $YBa_2Cu_4O_8$ using acetate and tartrate precursors. *Journal of Materials Chemistry*, 1994, **4**, 1267–1270.

14. Kareiva, A., Bryntse, I., Karppinen, M. and Niinistö, L., Influence of complexing agents on properties of $YBa_2Cu_4O_8$ superconductors prepared by the sol–gel method. *Journal of Solid State Chemistry*, 1996, **121**, 356–361.
15. Karppinen, M., Kareiva, A., Linden, J., Lippmaa, M. and Niinistö, L., Sol–gel synthesis and characterization of superconducting $(Y_{1-x}Eu_x)Ba_2(Cu^{57}_{1-y}Fe_y)_4O_8$ samples. *Journal of Alloys and Compounds*, 1995, **225**, 586–590.
16. Van Bael, M. K., Kareiva, A., Vanhoyland, G., Mullens, J., Franco, D., Yperman, J. and Van Poucke, L. C., Influence of calcium substitution on the formation and thermal stability of the $YBa_2Cu_4O_8$ superconductor. *Thermochimica Acta*, 1999, **340/341**, 407–416.
17. Van Bael, M. K., Kareiva, A., Vanhoyland, G., D'Haen, J., D'Olieslaeger, M., Franco, D., Quaeyhaegens, C., Yperman, J., Mullens, J. and Van Poucke, L. C., Enhancement of T_C by substituting strontium for barium in the $YBa_2Cu_4O_8$ superconductor prepared by a sol–gel method. *Physica C*, 1998, **307**, 209–220.
18. Van Bael, M. K., Kareiva, A., Nouwen, R., Schildermans, I., Vanhoyland, G., D'Haen, J., D'Olieslaeger, M., Franco, D., Mullens, J., Yperman, J. and Van Poucke, L. C., Sol–gel synthesis and properties of $YBa_2(Cu_{1-x}M_x)_4O_y$ (M = Co, Ni) and effects of additional replacement of yttrium by calcium. *International Journal of Inorganic Materials*, 1999, **1**, 259–268.
19. Er, G., Ishida, S. and Takeuchi, N., Investigations of the electrical property, diffuse reflectance and ESR spectra of the La-(Fe,Mn)-codoped PTCR $BaTiO_3$ annealed in reducing atmosphere. *Journal of Materials Science*, 1999, **34**, 4265–4270.
20. Brinker, C. J. and Scherrer, G. W., *Sol–Gel Science: The Physics and Chemistry of Sol–Gel Processing*. Academic Press, San Diego, 1990.
21. Callender, R. L., Harlan, C. J., Shapiro, N. M., Jones, C. D., Callahan, D. L., Wiesner, M. R., MacQueen, D. B., Cook, R. and Barron, A. R., Aqueous synthesis of water-soluble alumoxanes: environmentally benign precursors to alumina and aluminum-based ceramics. *Chemistry of Materials*, 1997, **9**, 2418–2433.
22. Veith, M., Mathur, S., Kareiva, A., Jilavi, M., Zimmer, M. and Huch, V., Low temperature synthesis of nanocrystalline $Y_3Al_5O_{12}$ (YAG) and Ce-doped $Y_3Al_5O_{12}$ via different sol–gel methods. *Journal of Materials Chemistry*, 1999, **9**, 3069–3079.
23. Rouessac, V., Wang, J., Provost, J. and Desgardin, G., Rapid synthesis of the Bi(Pb)-2223 110 K superconductor by the EDTA sol–gel method. *Journal of Materials Science*, 1996, **31**, 3387–3390.
24. Jensen, T. R., A new polymorph of $LiZnPO_4.H_2O$; synthesis, crystal structure and thermal transformation. *Journal of Chemical Society, Dalton Transactions*, 1998, 2261–2266
25. Kareiva, A., Harlan, C. J., MacQueen, D. B., Cook, R. and Barron, A. R., Carboxylate substituted alumoxanes as processable precursors to transition metal–aluminum and lanthanide–aluminum mixed metal oxides: atomic scale mixing via a new transmetalation reaction. *Chemistry of Materials*, 1996, **8**, 2331–2340
26. Livage, J., Henry, M. and Sanchez, C., Sol–gel chemistry of transition metal oxides. *Progress In Solid State Chemistry*, 1988, **18**, 259–341.
27. Blanchard, J., In, M., Schaudel, B. and Sanchez, C., Hydrolysis and condensation reactions of transition metal alkoxides: calorimetric study and evaluation of the extent of reaction. *European Journal of Inorganic Chemistry*, 1998, 1115–1127
28. Westin, G. and Nygren, M., On the formation of M_{2+}-Sb_{3+}-alkoxide precursors and sol–gel processing of M–Sb oxides with M = Cr, Mn, Fe, Co, Ni, Cu and Zn. *Journal of Materials Science*, 1992, **27**, 1617–1625.
29. Mullens, J., Vos, A., De Backer, A., Franco, D., Yperman, J. and Van Poucke, L. C., The decomposition of the oxalate precursor and the stability and reduction of the $YBa_2Cu_4O_8$ superconductor studied by TG coupled with FTIR and by XRD. *Journal of Thermal Analysis*, 1993, **40**, 303–311.
30. Pullar, R. C., Taylor, M. D. and Bhattacharya, A. K., The sintering behaviour, mechanical properties and creep resistance of aligned polycrystalline yttrium aluminium garnet (YAG) fibres, produced from an aqueous sol–gel precursor. *Journal of the European Ceramic Society*, 1999, **19**, 1747–1758.
31. Karppinen, M., Niinistö, L. and Yamauchi, H., Studies on the oxygen stoichiometry in superconducting cuprates by thermoanalytical methods. *Journal of Thermal Analysis*, 1997, **48**, 1123–1141.
32. Roy, S., Wang, L., Sigmund, W. and Aldinger, F., Synthesis of YAG phase by a citrate–nitrate combustion technique. *Materials Letters*, 1999, **39**, 138–141.
33. Niinistö, L., From precursors to thin films — thermoanalytical techniques in the thin film technology. *Journal of Thermal Analysis and Calorimetry*, 1999, **56**, 7–15.
34. Tautkus, S., Kazlauskas, R. and Kareiva, A., Thermogravimetric analysis — a powerful tool for the refinement of synthesis process of Hg-based superconductors. *Talanta*, 2000, **52**, 189–199.
35. Kareiva, A., Tautkus, S., Rapalaviciute, R., Jørgensen, J.-E. and Lundtoft, B., Sol–gel synthesis and characterization of barium titanate powders. *Journal of Materials Science*, 1999, **34**, 4853–4857.
36. Selvamanickam, V., Mironova, M., Son, S., Meyer, B. C. and Salama, K., Formation and phase decomposition of textured $YBa_2Cu_4O_8$ superconductor. *Physica C*, 1993, **217**, 113–120.
37. Karppinen, M., Linden, J., Valo, J., Kareiva, A., Kozlov, V., Terryll, K., Niinistö, L., Leskelä, M. and Rao, K. V., Iron substitution effects in $YBa_2Cu_4O_8$ synthesized by sol–gel technique. *Superconducting Science and Technology*, 1995, **8**, 79–84.
38. Lal, R., Pandey, S. P., Narlikar, A. V. and Gmelin, E., T_C depression in the $YBa_2Cu_{4-x}M_xO_8$ system for M = Fe, Ni, Zn, and Ga. *Physical Review B*, 1994, **49**, 6382–6384.
39. Karpinski, J., Kaldis, E., Jilek, E., Rusiecki, S. and Bucher, B., Bulk synthesis of the 81-K superconductor $YBa_2Cu_4O_8$ at high oxygen pressure. *Nature*, 1988, **336**, 660–662.
40. Tatsumi, M., Kawazoe, M. and Yamamoto, S., Synthesis of bulk superconductors $RBa_2Cu_4O_8$ (R = Tm, Er, Ho, Y, Dy and Gd) by a simple solid-state reaction method. *Physica C*, 1996, **262**, 261–265.
41. Zheng, X.-G., Kuriyaki, H. and Hirakawa, K., Synthesis of bulk $YBa_2Cu_4O_8$ and $Y_{1-x}Ca_xBa_2Cu_4O_8$ at 1 atm oxygen pressure. *Physica C*, 1994, **235**(240), 435–436.
42. Wada, T., Sakurai, T., Suzuki, N., Koriyama, S., Yamauchi, H. and Tanaka, S., Preparation and properties of superconducting $Y(Ba_{1-x}Sr_x)_2Cu_4O_8$. *Physical Review B*, 1990, **41**, 11209–11213.